Fuel 397 (2025) 135448

Contents lists available at ScienceDirect

Fuel

journal homepage: www.elsevier.com/locate/fuel

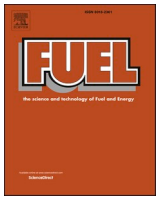

Full Length Article

Experimental and advanced numerical characterization of toluene fires

Benedetta Anna De Liso, Gianmaria Pio *, Ernesto Salzano

Department of Civil, Chemical, Environmental and Materials Engineering, Alma Mater Studiorum - University of Bologna, Bologna 40131, Italy

ARTICLE INFO

Keywords:
Consequence analysis
Pool fire
Cone calorimeter
Computational fluid dynamic
Detailed Kinetic mechanism

ABSTRACT

Toluene is employed in a variety of industrial applications worldwide being a largely adopted solvent and an active element in many products used in pharmaceutical, cosmetic, construction, paint, ink, and other industries. More recently, the use of this compound has been also suggested as a hydrogen carrier because of the implementation of the liquid organic hydrogen carrier (LOHC) strategy within the framework of the energy transition. In addition, the determination of the physico-chemical behavior of toluene can provide a positive impulse also for the representation of surrogate mixtures suitable for gasoline and diesel. The direct use of toluene as well as its consideration as a component of surrogate mixtures for fossil- and bio-derived fuels promotes accurate evaluations of its safety properties. In this work, an experimental campaign based on a modified procedure employing a cone calorimeter for the evaluation of mass and thermal properties of liquid toluene exposed to fire conditions is presented and compared with a numerical study employing a computational fluid dynamic (CFD) approach. The impacts of the kinetic sub-models were tested by comparing the estimated temporal and spatial distributions of temperature and exhaust composition assuming a reduced mechanism, a single-step infinitely fast reaction, and a hybrid approach. An excellent agreement among the implemented approaches was found, providing a robust database and model for the characterization of accidental scenarios involving toluene. Further insights on the flame structures and the phenomena ruling the pool fire of toluene were obtained, based on the utilization of the dedicated kinetic mechanism in CFD analysis. The strategies and assumptions posed to combine experimental and detailed numerical analyses can be also intended as a possible procedure for the characterization of the consequence analysis related to accidental releases of liquid substances.

1. Introduction

Several industrial processes utilize hydrocarbon solvents either to control the temperature of equipment items or to separate substances [1]. Among the others, toluene has been intensively adopted in industrial processes [2]. More recently, this compound has also been suggested as a promising liquid organic hydrogen carrier (LOHC) [3]. In addition, the determination of the physico-chemical behavior of toluene can provide a positive impulse also for the representation of surrogate mixtures suitable for gasoline and diesel [4]. Toluene is a toxic and flammable compound, having a boiling temperature of 110.6 °C and a flash point of 4 °C. Considering thermodynamic properties and overall reaction rate of toluene in air, in the case of accidental release, a pool fire represents the main concern together with flash fire [5]. This observation is supported by the analysis of past accidents that occurred in the chemical and process industries as well as during storage and transportation phases involving toluene [6,7]. As a way of example, according to the Occupational Safety and Health Administration (OSHA) [8] database on industrial accidents, a toluene flash fire has been recently reported in Motor and Generator Manufacturing in Massachusetts (Accident Summary Nr: 141079.015) and two accidents involving toluene pool fires have been described in Georgia (Accident Summary Nr: 200902575) and Tennessee (Accident Summary Nr: 200626067). In all cases, the source of ignition is unknown or poorly assessed. Nevertheless, most of the available literature covering the characterisation of mixtures containing toluene is oriented toward the assessment of the impact of its presence within exhaust gases on the environment or the normal operation of diesel engines [9] as well as the chemistry of liquid blends with other hydrocarbons (e.g., heptane, dodecane) in the view of surrogate mixtures [10,11]. Therefore, an in-depth analysis to evaluate the behaviour of liquid toluene exposed to an oxidative environment and fire conditions is highly desirable.

The characterization of pool fire has the quantification of mass burning rate (MBR) and power production rate as the main target [12]. For the scope of the consequence analysis of pool fires, most of the effort in the scientific and industrial communities is devoted to the realization of robust databases and models for the quantification of the

* Corresponding author.
E-mail address: gianmaria.pio@unibo.it (G. Pio).

https://doi.org/10.1016/j.fuel.2025.135448
Received 30 December 2024; Received in revised form 17 April 2025; Accepted 18 April 2025
Available online 24 April 2025

Nomenclature (* Units of the pre-exponential factor depend on the reaction kinetic order. All considered reactions have elementary kinetics and units are in mol, l, and s.)

Symbol	Definiton, Unit
A	Pre-exponential factor, *
B	Spalding mass tranfer number, [-]
C_p	Specific heat of the air, [kJ/kg•K]
D	Characteristic diameter, [m]
e	Specific internal energy, [J/kg]
E_a	Activation energy, [kcal/mol]
f	Body force per unit mass, [N/kg]
g	Gravitational acceleration, [m/s]
h	Mass transfer coefficient, [kg/m^2•s]
HRR	Heat Release Rate, [kW/m^2]
HRR*	Dimensionless Heat Release Rate, [–]
HRR_s	Heat Release Rate at steady state condition, [kW/m^2]
HRR_t	Total Heat Release Rate, [kW/m^2]
I	Identity tensor, [–]
MBR	Mass Burning Rate, [g/s]
MBR*	Dimensionless Mass Burning Rate, [–]
MBR_s	Mass Burning Rate at steady state condition, [g/s]
p	Pressure, [Pa]
q	Heat flux vector, [W/m^2]
t	Time, [s]
t*	Dimensionless time, [–]
T_a	Ambient temperature, [K]
t_s	Time to reach steady state conditions, [s]
v	Velocity vector, [m/s]
δ	Cell size, [cm]
λ	Second viscosity coefficient, [Pa • s]
μ	Viscosity, [Pa • s]
ρ	Density, [kg/m^3]
ρ_a	Density of the air, [kg/m^3]
ρ_f	Density of the liquid film, [kg/m^3]
τ	Viscous stress tensor, [Pa]
$x_{tol,s}$	Mass fraction of toluene on the liquid surface, [–]
$y_{tol,g}$	Mass fraction of toluene in the gas phase, [–]

abovementioned parameters at steady-state conditions to determine the possible occurrence of second cascading events [13]. These parameters are significantly influenced by the pool size at steady-state conditions, being determinant for the fluid dynamic regime of diffusive flames [14]. In this sense, it is worth mentioning the empirical correlations reported within the pioneering work of Hottel [15] for the estimation of the mass burning rate and the flame height as a function of the pool diameter. The flame height is typically intended as the upper bound of the heat release, characterized by the transition from reactive to non-reactive plume [16]. Quite obviously, it is potentially affected by the unsteady fluctuations and turbulence intrinsically characterizing the diffusion flames. However, the flame height can be evaluated based on the values at 50 % intermittency [17]. Several correlations have been developed for the quantification of this parameter based on the pool size, fuel properties, and environmental conditions. As a way of example, the pioneering studies reported by Thomas [18] proposed a correlation accounting for the mass burning rate, pool diameter, density of air, and gravitational acceleration to estimate the ratio between flame height and diameter. More recently, Heskestad (2002) [19] presented an empirical correlation based on a variety of experimental data estimating the ratio between flame height and diameter as a function of the heat release rate. Similarly, several correlations have been developed to estimate the temperature distribution at the centerline based on the flame intensity and atmospheric conditions. Among the others, the Heskestad [19] and McCaffrey [20] correlations are worth to be mentioned although it is also important to note that their accuracy can be limited for distances below the flame height. Besides, the a priori identification of the conditions resulting in the transition from different flame regimes is still challenging since it is affected by the physical and chemical properties of the investigated compound or mixture, promoting dedicated studies. To this scope, either experimental or numerical approaches can be employed.

For what concerns the experimental studies, results suffer from the lack of rigorous and standardized procedures allowing for the comparison of data deriving from different campaigns. As a way of example, the variability in boundary conditions (e.g., pool thickness, existence of backup flowrate, atmospheric conditions, wind speed, and velocity), possibly resulting from the analysis of open-field large-scale scenarios, has been indicated as a major issue for a successful comparison of experimental databases [21]. Conversely, pool fires of small and bench scales of toluene under a controlled atmosphere and set of boundary conditions have been analyzed in the literature [11,22], with a specific focus on the temperature distribution in the proximity of the flame and the soot formation. Recently, the possibility of employing a standardized system for the bench-scale analysis (i.e., a cone calorimeter) of the flame behavior and ignitability of liquid compounds has been proposed [23], allowing for the evaluation of the effects of external heat flux on the most relevant parameters for the characterization of a pool fire (e.g., heat release rate and mass burning rate) as well as to the determination of the yields for the main products (i.e., CO, CO_2, and soot) [24].

The availability of a robust and dedicated experimental database can have beneficial effects on numerical studies, as well. Indeed, it can serve as a source of validation for advanced models or input for simplified approaches. In this sense, it is worth considering the possible strategies available for the evaluation of the chemistry of reactive systems in computational fluid dynamics (CFD), as reported in a recent review [25]. More specifically, CFD software typically offers the possibility to represent the chemistry of the analyzed system as a single-step reaction, having empirical correlations and/or yield values to determine the overall reactivity and the exhaust composition. Alternatively, detailed kinetic mechanisms (once reduced) can be included in CFD studies, allowing for the identification of the most relevant intermediates and the quantification of their production and consumption rates. Recently Chen et al. (2023) [16] have indicated the realization of models combining chemistry (including soot formation), fluid dynamics, heat, and mass transfer as the main challenge in pool fire characterization. In addition, Lu and Law (2009) [26] suggested the implementation of realistic fuel chemistry in large-scale calculations devoted to the representation of pool fire. In this case, the initial detailed kinetic mechanisms can contain ~100 species and ~1000 reactions, thus they must be reduced significantly to guarantee a successful implementation [27]. Typically, the target size is ~10 species ~30 reactions [28]. This approach includes additional equations to be solved, with obvious implications on the computational requirements. However, it represents a flexible feature for the characterization of the analyzed scenario as well as it is the only strategy providing information on the exhaust composition, even in the absence of specific data.

For these reasons, this work presents a combination of experimental and numerical analysis aiming at the characterization of the main parameters involving pool fire. To this aim, a detailed kinetic mechanism was introduced into the numerical analysis. The obtained estimations were compared with experimental measurements for the sake of validation. The combination of different approaches provided a powerful feature for the characterization of reactive systems involving toluene, paving the way to design optimization and process intensification as well as toward a robust evaluation of the safety and sustainability of

industrial processes.

2. Methodology

The current work presents either an experimental campaign or a numerical investigation devoted to the characterization of fire-related scenarios associated with a possible release in the atmosphere of toluene. Considering the different nature of the adopted strategies, the methodological section was divided into two subsections, accordingly.

2.1. Experimental approach

The experimental tests reported in this work were conducted on a cone calorimeter to evaluate the bench scale behavior of toluene under a wide range of conditions representative of possible accidental releases of liquid substances. The cone calorimeter is conventionally used for the analysis of solid materials [29], however, in this study, it was employed to characterize the combustion behavior of liquid samples. The apparatus consists of a truncated conical radiant heater designed to deliver a precisely controlled and uniform heat flux to the sample surface. The sample is contained in a stainless-steel sample holder (100 × 100 mm) and positioned on a high-precision load cell to continuously monitor the mass of the liquid sample throughout the test. Ignition is achieved using a high-voltage (10 kV) electrical spark igniter, ensuring reliable and reproducible ignition conditions. The entire setup is housed under a well-calibrated exhaust hood, equipped with an air supply system providing a controlled and almost constant flow rate of 24 L/s to maintain steady-state combustion conditions and facilitate the collection of combustion by-products. Guaranteeing a constant flowrate is essential since the air entrainment in post-flame and plume regions can potentially affect the mixing rate of combustible gas and air, thermal phenomena, and fluid-dynamic regimes with potential implications on the resulting mass burning rate, heat release rate, and exhaust gas composition (e.g., CO formation), as discussed in detail in dedicated studies available in the current literature [30]. Although variations in exhaust composition and temperature can make this process challenging from a practical perspective, the continuous measurements of stack and smoke temperatures, composition, and differential pressure limited the variability of the flow rate throughout the experimental campaign within the range of 24 ± 0.5 L/s. This value guarantees a negligible impact on the measured properties according to previous investigations on the subject reported by Mun et al. (2021) [31]. The heat release rate (HRR) is determined through oxygen consumption calorimetry, leveraging the principle that 13.1 MJ of energy is released per kilogram of oxygen consumed during the combustion of hydrocarbons. This is achieved by continuously analyzing the oxygen depletion in the exhaust gases using a paramagnetic sensor, while additional gas analyzers measure CO and CO_2 concentrations to evaluate combustion efficiency and toxic emissions. The collected measurements were reported with a frequency of 1 Hz. A photometric laser beam system is used to monitor soot and particulate emissions, offering further insight into the combustion characteristics of toluene. Calibration procedures are meticulously carried out before each test to ensure accuracy and repeatability. The radiant heater output is verified using a heat flux gauge placed at the sample position to confirm the delivered thermal load. The load cell is tared and validated using certified reference weights to ensure precise mass measurements. The exhaust flow rate is calibrated using a reference orifice plate flowmeter, while the gas analyzers are calibrated using standard span gases with known compositions, guaranteeing compliance with international fire testing standards (e.g., ISO 5660, ASTM E1354) and ensuring high fidelity in the obtained experimental data. A schematic representation of the described system is reported in Fig. 1, whereas additional information on the geometrical features and material properties of the cone calorimeter can be found elsewhere [32,33].

Toluene having a purity of >99 %w was analyzed once exposed to air and heat fluxes between 7 and 50 kW/m^2. Conversely, a sample surface of 0.01 m^2, an initial sample thickness of 0.01 m, and a distance between the sample and the horizontally oriented cone heater of 0.025 m were kept constant for all the tests. The ignition source was provided at the beginning of each test. A detailed description of the experimental procedure implemented in this work can be found in previous work from the same authors, addressing the characterization of liquid substances [24].

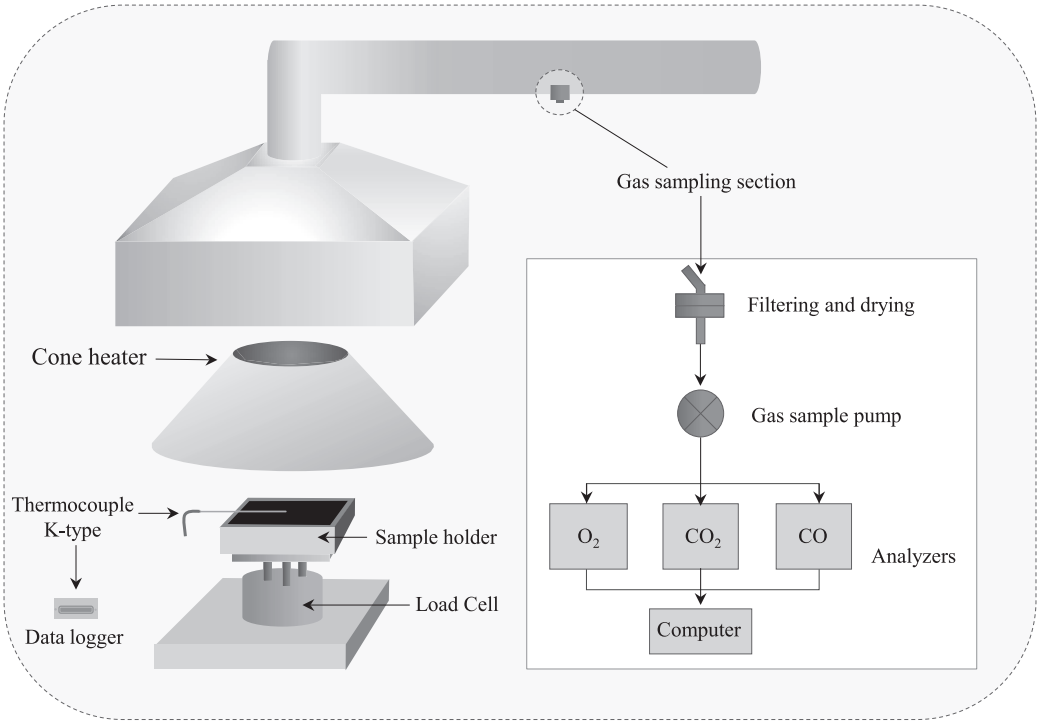

Fig. 1. Schematic representation of the experimental system adopted in this work.

2.2. Numerical approach

The open-source software Fire Dynamic Simulator (FDS) [34], developed by the National Institute of Standards and Technology (NIST), was adopted for the numerical analysis carried out in this work. Continuity conservation, momentum conservation, and energy conservation equations were implemented together with the definition of stress tensor, according to the classical definition for Navier-Stokes equations for Newtonian fluids, as reported below:

$$\frac{\partial \rho}{\partial t} + \nabla\cdot(\rho \mathrm{v}) = 0 \tag{1}$$

$$\frac{\partial \rho \mathrm{v}}{\partial t} + \mathrm{v}\cdot\nabla\rho\mathrm{v} = -\nabla \mathrm{p} + \nabla\cdot\tau + \rho \mathrm{f} + \nabla\cdot(\rho \mathrm{v}) = 0 \tag{2}$$

$$\frac{\partial \rho \mathrm{e}}{\partial t} + \mathrm{v}\cdot\nabla\rho\mathrm{e} = -\nabla\cdot\mathrm{q} + \tau : \nabla \mathrm{v} + \rho \mathrm{f}\cdot\mathrm{v} \tag{3}$$

$$\tau = \mu\left(\nabla \mathrm{v} + (\nabla \mathrm{v})^{\mathrm{T}}\right) - \left(\lambda - \frac{2\mu}{3}\right)\mathrm{I}\nabla\cdot\mathrm{v} \tag{4}$$

where ρ is the density, v is the velocity vector, p is the pressure, τ is the viscous stress tensor, f is the body force per unit mass, e is the specific internal energy, q is the heat flux vector, μ is the viscosity, λ is the second viscosity coefficient, and I is the identity tensor. The evaporation rate ($\dot{m}''$) of the pool was estimated by using Eq. (5), where the mass transfer coefficient (h), film density (ρ_f), Spalding mass transfer number (B), the mass fraction of toluene on the liquid surface ($x_{tol,l}$), and the mass fraction of toluene in the vapor phase on the cell adjacent to the liquid surface ($y_{tol,g}$) were employed and defined in agreement with the technical reference guide of FDS [35].

$$\dot{m}'' = \mathrm{h}\,\rho_f \ln(1+B)\frac{\left(x_{tol,s}(B+1) - y_{tol,g}\right)}{B} \tag{5}$$

The turbulent mass and thermal diffusivities were calculated assuming constant Schmidt and Prandtl numbers, respectively, and using the sub-grid scale kinetic energy included within Deadorff's model, following the specifications provided by dedicated literature [36]. A calm atmosphere, free mass, and heat transfer through lateral and upper surfaces were considered. A parallelepiped pool of toluene having the dimensions of 10 cm × 10 cm × 2 cm was defined, in line with the experimental setup described in the previous section. Based on the time resolution, the sampling frequency considered for the numerical investigation was ~10 Hz. A domain of 40 cm × 40 cm × 80 cm was considered to avoid a potential interaction between the observed phenomena and posed boundary conditions on the external faces (Fig. 2).

The defined computational domain was divided into a structured cubic-shaped grid, having an average cell size (δ) of 0.5 cm, in agreement with the ratio between the cell size and pool diameter suggested by previous grid sensitivity studies on aromatic containing pool fires comparing the estimation of the time evolution of heat flux for different mesh definitions [37]. Besides, the selected value is in line with the criterion D/δ > 16 for the definition of a fine mesh typically adopted for numerical studies involving fires in FDS [38], calculating the characteristic diameter D as reported in Eq. (6).

$$D = \left(\frac{HRR_t}{\rho_a c_p T_a g^{0.5}}\right)^{\frac{2}{5}} \tag{6}$$

where HRR_t is the total heat release rate of the fire, whereas ρ_a, c_p, T_a and g are the density of the air, specific heat of the air, ambient temperature, and gravitational acceleration, respectively. Two different strategies were considered for the chemical sub-model: simple chemistry and detailed kinetic mechanism. The former option implies a single and infinitely fast chemical reaction limited by mixing phenomena, whereas the latter is based on the implementation of a detailed kinetic mechanism in a reduced form. Within the framework of simple chemistry, complete oxidation of toluene to steam and carbon dioxide was considered at first. Then, the incomplete oxidation (Equation (7) to form carbon monoxide and the formation of soot were considered, assuming yields of 0.1 and 0.14, respectively.

$$C_7H_8 + \nu_{O_2}O_2 \rightarrow \nu_{CO_2}CO_2 + \nu_{H_2O}H_2O + \nu_{CO}CO + \nu_{Soot}Soot \tag{7}$$

The reported values are selected in line with the experimental observations once an external heat flux of 15 kW/m^2 was provided to the surface of the sample. In this sense, it is worth noting that, based on the simple chemistry definition, the external heat flux and the ignition source were not necessary to produce a stable flame, thus, they were not included within the numerical domain at this stage. For what concern the kinetic mechanism, previous works have been devoted to the reduction of detailed mechanisms for toluene oxidation under flame-relevant conditions [37]. To this scope, a combination of rate of production analysis, for the selection of the most relevant paths, and sensitivity analyses, for the identification of the reactions mostly affecting the abovementioned branches, has been implemented. This procedure has two main targets to make the adoption of a kinetic mechanism in CFD analysis feasible: (i) the production of a list of overall apparent reactions leading to the formation of the main products and intermediate species and (ii) the identification of the rate-determining steps corresponding to each overall apparent reactions. For the sake of completeness, the list of the rate-determining steps and the corresponding kinetic coefficients considered for the numerical analysis is reported in Table 1. The main products and stable intermediates

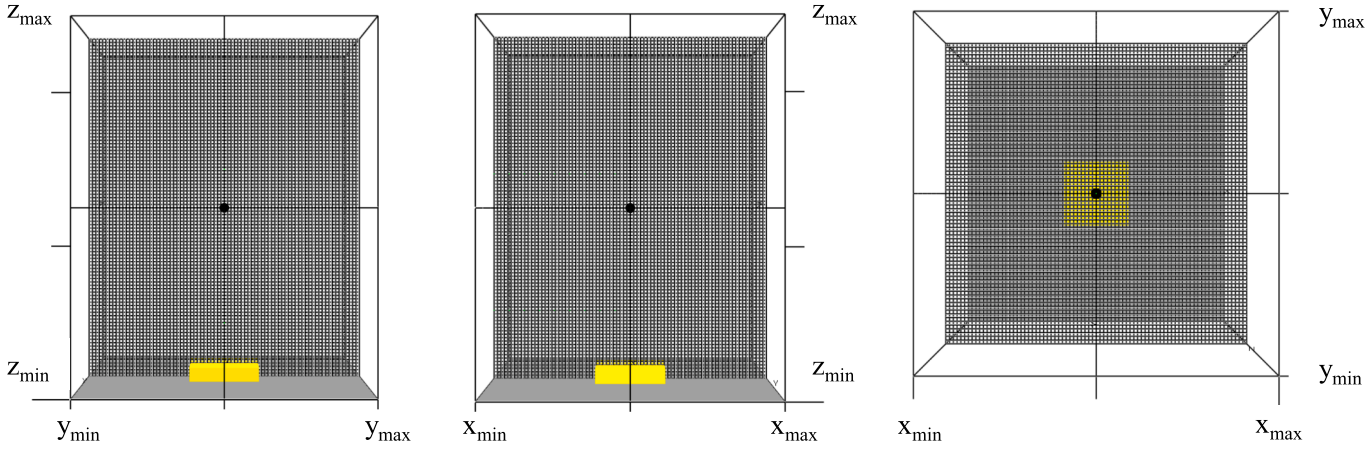

Fig. 2. Representation of the numerical domain adopted in this work from the x_{max} (left), y_{max} (center), and z_{max} (right) perspectives.

Table 1
Reactions and kinetic parameters considered as the rate determining steps for the numerical investigation performed in this work, as reported by dedicated studies on the chemistry of toluene-containing mixtures [37].

Reaction #	Formula	A [*]	E_a [kcal/mol]	b [-]
1	$C_7H_8 \rightleftharpoons C_6H_5 + CH_3$	$1.2 \bullet 10^{16}$	$1.0 \bullet 10^{2}$	0
2	$CH_3 + H + (M) \rightleftharpoons CH_4 + (M)$**	$6.4 \bullet 10^{23}$; $1.2 \bullet 10^{15}$	0.0; 0.0	−0.4; −1.8
3	$CH_3 + HCO \rightleftharpoons CH_4 + CO$	$1.0 \bullet 10^{14}$	0.0	0.0
4	$H_2 + 0.5O_2 \rightleftharpoons H_2O$	$2.3 \bullet 10^{14}$	17	0.0
5	$2O \rightleftharpoons O_2$	$1.6 \bullet 10^{14}$	120	0.0
6	$CH_3 + 2O_2 \rightleftharpoons CO_2 + 2H_2O$	$1.3 \bullet 10^{13}$	1.5	0.0
7	$2H \rightleftharpoons H_2$	$2.2 \bullet 10^{14}$	96	0.0
8	$CH_4 + O_2 \rightleftharpoons CO + 2H_2 + O$	$1.6 \bullet 10^{13}$	1.5	0.0
9	$CO + H_2O \rightleftharpoons CO_2 + H_2$	$2.0 \bullet 10^{11}$	38	0.0
10	$C_7H_8 \rightleftharpoons C_4H_5 + C_3H_3$	$1.0 \bullet 10^{12}$	80	0.0
11	$C_7H_7 \rightleftharpoons C_6H_4 + CH_3$	$1.0 \bullet 10^{12}$	80	0.0
12	$C_6H_4 \rightleftharpoons C_2H_2 + C_4H_2$	$1.0 \bullet 10^{12}$	80	0.0

* Units of the pre-exponential factor depend on the reaction kinetic order. All considered reactions have elementary kinetics and units are in mol, l, and s.
** Third body reaction

considered in this work were carbon dioxide, carbon monoxide, water, soot, methane, and hydrogen. It is worth mentioning that species can be produced by different reaction branches. As a way of example, the formation of soot was assumed instantaneous once soot precursors such as C_2H_2 and C_3H_3 were formed. In addition, the production of a given species or intermediates can be the results of a series of rate-determining steps included in the list, as in the case of C_2H_2 formation which results from the H abstraction from toluene followed by C–C break bond represented by R11 and R12.

In contrast with the simulations implementing the simple chemistry, two different cases in terms of external heat flux and ignition source were tested once the kinetic mechanism was considered. More specifically, in one case external flux and ignition source were not considered, in line with the set of boundary conditions imposed for the simple chemistry simulations, whereas in another case a given and constant external flux of 15 kW/m^2 was assumed on the liquid surface in line with the experimental condition considered and an impulse ramp reaching the maximum temperature of 1200 K in 0.1 s was applied to a cubic element (size 0.005 m × 0.005 m × 0.005 m) in the proximity of the pool border to simulate the ignition source. For the sake of clarity, Table 2 reports the set of conditions tested.

Regardless of the implemented strategy, the temporal evolution of the heat release rate, the mass burning rate, and the spatial distribution of the temperature within the domain were monitored and compared. Additional elements were collected for the case of the implementation of the kinetic mechanism related to the exhaust composition and the distribution of relevant intermediates.

Table 2
Summary of the main differences between the numerical simulations performed in this work.

Case #	Chemistry	CO & Soot Yields	Ignition source	External heat flux
1	Simple Chemistry	No	No	No
2	Simple Chemistry	Constant value	No	No
3	Kinetic Mechanism	Calculated	Constant value	Constant value
4	Kinetic Mechanism	Calculated	No	No

3. Results and discussion

Considering the typical evolution of a pool fire without a continuous backup flow rate, the obtained data were distinguished to focus on the growth phase (Fig. 3) and pseudo-steady-state (Table 3) regime. The growth phase is intended as the time interval from the beginning of the test to the achievement of a stable value of HRR, thus it is different in each case analyzed in this work. Therefore, to enable a more effective comparison between experimental and numerical results, dimensionless quantities were introduced for both the HRR and the MBR. The dimensionless heat release rate is defined as $HRR^* = HRR / HRR_s$, where HRR_s represents the steady-state heat release rate. Likewise, the dimensionless mass burning rate is given by $MBR^* = MBR / MBR_s$, with MBR_s denoting the steady-state value of the MBR. Time has also been normalized as $t^* = t / t_s$, where t_s is the time required to reach the steady-state combustion regime. Fig. 3 illustrates the evolution of HRR* (left) and MBR* (right) as functions of t*, highlighting the transient and steady-state phases of the combustion process. This normalization allows for a clearer assessment of combustion dynamics, independent of absolute values, and facilitates the evaluation of numerical model accuracy in predicting both ignition transients and steady-state behavior.

It is worth noting that, only data deriving from the Case 1, Case 2, and Case 3 were reported in this section for the numerical analysis together with the experimental data collected in this work. Indeed, once the kinetic mechanism was implemented in the absence of an ignition source and external heat flux (i.e., Case 4) no flame was observed and consequentially toluene evaporation and dispersion were noted without the formation of a stable flame. In other words, the boundary conditions and models implemented for Case 4 cannot be considered for the evaluation of pool fires, but they offer the possibility to accurately evaluate alternative scenarios, such as flash fires. Considering that the room temperature is significantly lower than the autoignition temperature, the dispersion scenario better represents the real case once no heat flux and ignition are provided. Conversely, the adoption of simple chemistry (i.e., Case 1 and Case 2) implies that an effective ignition source is always available if fuel and oxidant are present in a sufficient amount. Therefore, it is possible to infer that the implementation of a kinetic mechanism offers the additional potential advantage of intrinsically distinguishing the flammable from the non-flammable set of boundary conditions.

The experimental HRR curve exhibits a characteristic growth phase starting around $t^* \approx 0.4$, followed by a rapid increase leading to a peak at approximately $t^* \approx 0.8$. Although the curve is marked by oscillations in the fully developed phase, likely due to flame intrinsic instabilities and turbulent mixing effects of the investigated flames, all the values are included within the range of ±5 % of the time-averaged value and similar frequencies can be observed for the numerical models employed in this work. Similarly, the MBR trend follows a comparable progression, showing a delayed ignition phase, a steep increase, and a final stabilization. The onset of significant liquid consumption occurs slightly later than the HRR rise, suggesting a thermal lag between fuel evaporation and combustion onset. Both curves ultimately reach a steady-state regime before the burnout phase. Noteworthy, HRR* and MBR* profiles are almost perfectly reproduced by Case 3 either in terms of ignition behavior or flame intensity, providing significant support for the validation of the adopted models. The numerical HRR and MBR profiles show similar trends in terms of growth and steady-state values for Case 1 and Case 2. Conversely, a sharper increase can be observed in Case 3 for both profiles, meaning that the initiation reactions included in the kinetic mechanism have faster kinetics than the simple chemistry included in the FDS database under the investigated conditions. This observation can be attributed to the production of smaller molecules from the C–C bond brake of toluene, leading to faster mixing with oxygen and overall kinetics for exothermic reactions. Once the steady state is reached, HRR and MBR values obtained in Case 3 slightly differ from the other numerical cases. More specifically, the HRR is between the estimations

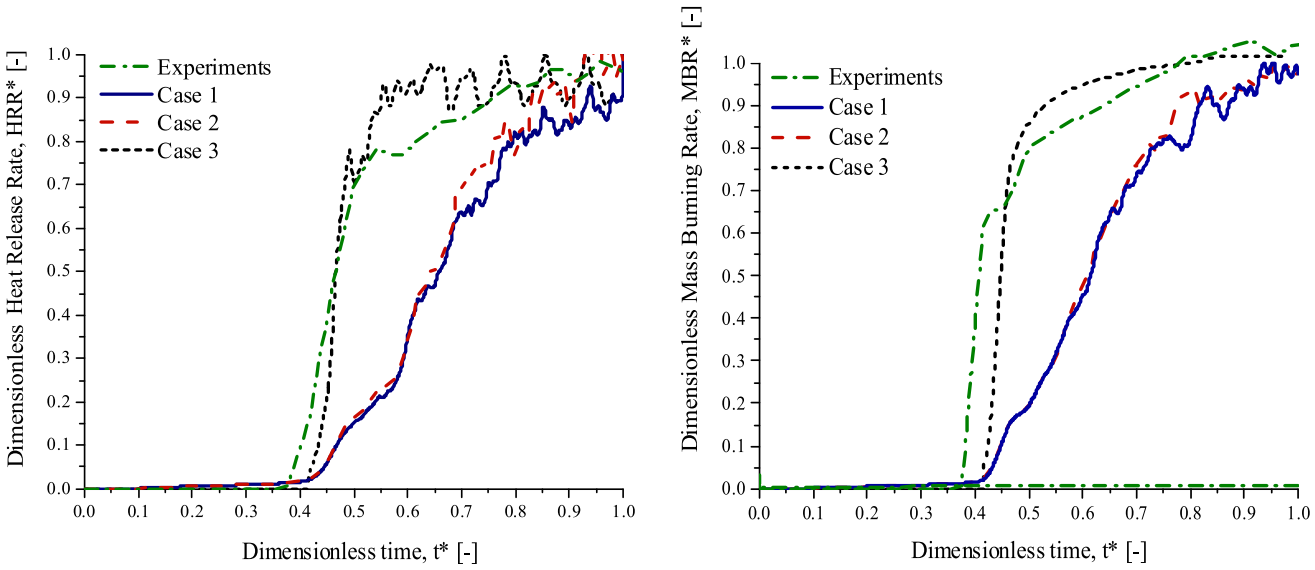

Fig. 3. Time evolution of the dimensionless heat release rate (left) and dimensionless mass burning rate (right) obtained in this work from a bench-scale pool fire of toluene, as a function of the approaches adopted.

Table 3
Heat release rate, mass burning rate, and soot yield obtained by the numerical and experimental analyses. Oscillation frequencies were also added for the numerical cases.

Approach	HRR_s [kW/m^2]	MBR_s [g/s]	Y_{soot} [kg/kg]	Oscillation frequency [Hz]
Case 1	2110	0.54	0.000*	2.28
Case 2	1956	0.54	0.140*	2.05
Case 3	2058	0.57	0.144	2.35
Experiments	2097	0.58	0.140	Not measurable

* = The reported value is included as input.

obtained for Case 1 and Case 2, whereas MBR is the largest among numerical data and the closest to the experimental measurements. The combination of these trends implies that a less effective combustion process derives from the utilization of the detailed kinetic mechanism since the increased availability of toluene in the vapor phase is not proportional to the estimated HRR. In other words, the overall heat of the apparent reaction resulting from the ratio between HRR and MBR can be sorted as Case 1 > Case 2 > Case 3. This consideration is supported by the conveyed soot yields, showing slightly larger values for Case 3.

A comparative analysis of the results obtained from Case 1 and Case 2 revealed a high degree of similarity in terms of both calculated HRR and the MBR values. Quite obviously, slightly lower values for HRR at steady state and maximum temperature can be observed for Case 2, although the estimated MBR is consistent between the two approaches. These discrepancies are associated with the incomplete oxidation of toluene toward the formation of carbon monoxide and soot. More specifically, the reduction of HRR can be quantified as ~7 % between the two simple chemistry approaches. Nevertheless, the variation in produced heat observed in this study has a negligible effect on the MBR, which is determined by the evaporation and mixing phenomena. Hence, while minor discrepancies were observed between these methods, these were generally within acceptable margins and did not significantly impact the overall conclusions drawn from the analysis once the thermal aspects were of concern. Conversely, if the quality of the air is relevant for a specific investigation (e.g., once fires are expected in a poorly ventilated or closed environment), data deriving from Case 2 can be more effectively compared with the ones deriving from Case 3. Considering the chemical structure assumed for the soot particles (i.e., $C_{18}H_2$) and the composition estimated at the time and location where the maximum molar fraction of soot was observed, the maximum soot yield corresponds to 0.144. This value is in excellent agreement with homologous data deriving from the experimental campaign reported in the current literature [24] and also adopted as an input for Case 2, demonstrating the ability of the kinetic mechanism to predict the exhaust composition adopting only theoretically derived coefficients. Overall, the numerical models exhibit good agreement with the experimental data, particularly in capturing the overall evolution of HRR and MBR. Case 1 closely follows the experimental curve in both the acceleration and steady-state phases, successfully reproducing the peak values and fluctuations observed in HRR. Case 2 slightly underestimates the initial rise rate, indicating a difference in the predicted ignition dynamics. Case 3 aligns well with the experimental trend but exhibits higher fluctuations in the HRR profile. In the MBR plot, the models show a similar progression to the experimental data, though some deviations in the early-stage growth rate suggest potential discrepancies in the evaporation kinetics or thermal feedback mechanisms. Hence, the numerical approaches effectively capture the dominant combustion characteristics, demonstrating their robustness in predicting pool fire behavior for toluene. In this sense, it is worth noting that the flame geometry is well captured by the numerical estimations, as well. Indeed, based on the measured MBR and HRR at the steady-state, the flame heights respectively resulting from Thomas [18] and Heskestad [19] correlations are 0.64 m and 0.69 m, which almost perfectly align with the time-averaged flame height estimated for Case 3 being equal to 0.68 m. The agreement between experimental and numerical data can be intended as a further demonstration of the validity of the implemented models.

Additional considerations can be obtained based on the comparison of the temperature distribution at steady-state conditions obtained by the different numerical strategies implemented in this work (Fig. 4). To guarantee a meaningful comparison, the reported temperature distribution data refer to the same instant, selected as 10 s, to guarantee that a stable steady-state regime was achieved for all the numerical approaches. Similarly, numerical predictions of the distribution of the centerline temperature resulting from Case 1, Case 2, and Case 3 were compared with the estimations from Heskestad and McCaffrey correlations (Table 4).

The comparison of the temperature profiles indicates that Case 3 provides the most accurate representation of the trend established by well-known correlations. Specifically, the predictions from Case 3 show

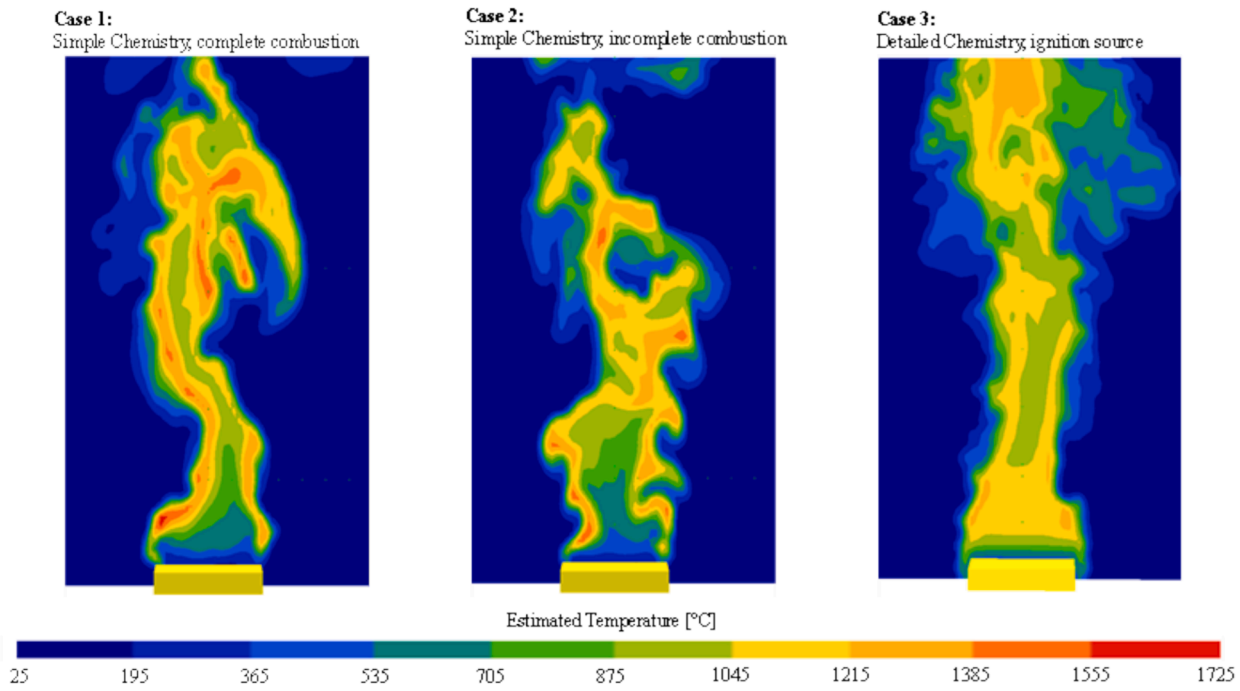

Fig. 4. Spatial distribution of the estimated temperatures at steady-state conditions, as obtained for Case 1 (left), Case 2(center), and Case 3 (right).

Table 4
Distribution of the centerline temperature as a function of the distance from the liquid pool obtained from numerical models and empirical correlations.

Distance [m]	Centerline temperature [K]				
	Case 1	Case 2	Case 3	Heskestad	McCaffrey
0.4	1425.3	896.5	1117.6	1173.5	869.6
0.5	1070.0	799.9	898.3	901.6	755.3
0.6	824.7	660.1	761.1	743.4	679.1
0.7	762.0	525.0	665.0	642.5	610.6
0.8	713.4	431.0	578.0	573.8	548.3

all deviations within ±5 % of those derived from Heskestad's correlation, whereas larger discrepancies are observed for Case 1 and Case 2, reaching up to +25 % and −25 %, respectively. As expected, Case 1 tends to overestimate the temperature values, whereas Case 2 underestimates the temperatures, in line with the assumptions of complete combustion (Case 1) and uncomplete (Case 2) combustion. Although larger discrepancies can be observed between numerical estimations obtained in this work and McCaffrey's correlation, especially in the intermittent region (i.e., for $z/HRR^{0.4}$ within 0.08 and 0.2), the same trend between numerical approaches can be detected. Therefore, it is possible to conclude that, in contrast with the simple chemistry approach (i.e., Case 1 and Case 2), the utilization of kinetic mechanism in CFD analysis allows for in-depth evaluation of the flame structure and the identification of specific areas within the flame: (*i*) a toluene-rich

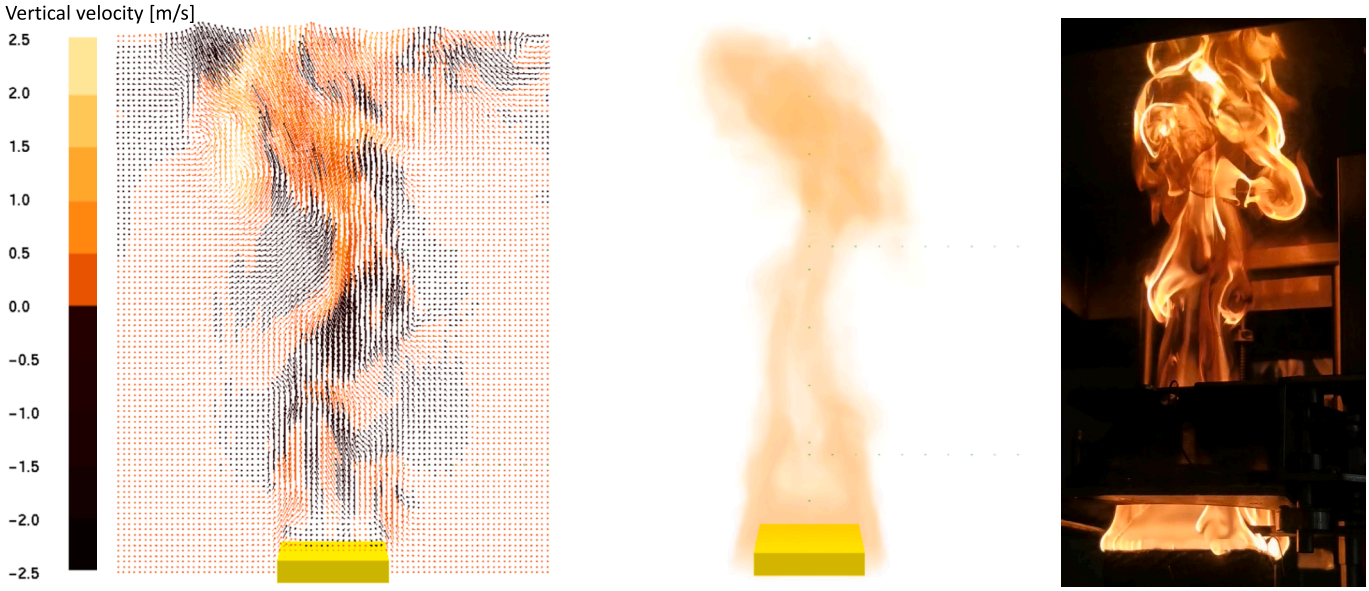

Fig. 5. Numerical simulation of the cone calorimeter test of a toluene pool fire under a heat flux of 15 kW/m^2 in terms of vertical velocity (left), flame shape (center), and comparison with the experimental test conducted through cone calorimeter (right).

vapor layer in the proximity of the liquid pool, with a partial overflow from the vertical projection of the sample holder, in agreement with the flame structure depicted experimentally under the same boundary conditions (Fig. 5), (*ii*) a pyrolysis dominated area where small species (e.g., methyl radical and hydrogen atom) and radicals (e.g., phenyl) are produced from toluene, (*iii*) a high-temperature reacting area where carbon monoxide and carbon dioxide formations are ruling the chemistry of the system once enough oxygen content is locally available or, conversely, soot precursors are formed in the case of oxygen limitation, (*iv*) an area characterized by soot formation and hot gas diffusion. The possibility to accurately reproduce the flame geometry (e.g., flame height and surface) and intensity (e.g., temperature distribution) demonstrated by the assumptions posed for Case 3 promotes its utilization also for the determination of consequences in releasing conditions where these parameters are paramount [39,40].

Considering the structure of the adopted kinetic mechanism and the described flame zones, the combustion processes can be attributed to the pathways starting from methane and methyl radical, distinguishable from the pyrolysis pathways. Hence, an additional case assuming the detailed chemistry for the soot, methane, and methyl radical formation integrated with simple chemistry for methane was tested. It is worth noting that in this case, soot formation from methane was neglected, to avoid a double counting. This strategy is referred to as hybrid from now on. The results obtained from the implementation of the hybrid strategy show an almost perfect match between the obtained results. The main advantage of the hybrid strategy proposed in this work is related to the availability of a large set of data for the characterization of methane chemistry, allowing for the utilization of robust yield values [41,42] regardless of the initial fuel considered. Therefore, this approach lays the foundation for the inclusion of the rate-determining combustion/pyrolysis mechanisms leading to the formation of light components for the characterization of the chemistry of larger species. Hence, this approach represents a promising alternative to reduce the number of reactions to be included as well as to facilitate the studies of liquid and solid species. Indeed, most of the kinetic analysis on the chemistry of condensed species is focused on the determination of apparent kinetics for the formation of relevant compounds playing an essential role within the decomposition process [43]. In this sense, based on the source considered (e.g., fossil-derived or bio-based), common intermediates can be identified, such as light alkanes, light alkenes [44], organic acids, or alcohols [45]. Therefore, the existing databases on apparent reactions relevant to condensed phases can be integrated with reduced mechanisms mimicking the chemistry of key intermediates in the gaseous phase, coupling different databases and expertise in a single comprehensive numerical approach.

4. Conclusion

This work presents a detailed investigation of the chemistry of bench-scale pool fire resulting from the ignition of toluene. To this scope, different strategies for the evaluation of the chemistry of condensed fuels under an oxidative environment, including simple chemistry, detailed kinetic mechanism, and an innovative hybrid model, were compared in a computational fluid dynamic study. The obtained time evolution and spatial distribution of temperature and exhaust composition were successfully compared with experimental results derived from a dedicated experimental study on a cone calorimeter. Although the validation is performed for bench scale tests only, considering the nature of the adopted models, their accuracy can be also considered for industrial-relevant scales. The effects of yields for carbon monoxide and soot were analyzed for the case of simple chemistry, showing that soot formation has a limited impact on the overall heat release rate under the investigated conditions. The reduced kinetic mechanism implemented in this work was able to accurately predict the soot yield deriving from experimental results as well as the ignitability of toluene, as confirmed by the absence of a stable flame once external ignition sources were not provided within the numerical domain. Quite obviously, the inclusion of a kinetic mechanism, although in a reduced form, significantly increases the computational requirements. Therefore, the identification of the most convenient approach between simple chemistry and kinetic mechanism remains a specific task depending on the size of the fire (i.e., the utilization of kinetic mechanism is discouraged for large fires) and the target of the analysis (e.g., simple chemistry can be inadequate to predict the composition of pollutants). An almost perfect match between results obtained by the implementation of a detailed kinetic mechanism (reduced) and a hybrid model combining detailed chemistry for the production of soot, methane, and methyl radical with simple chemistry for methane and methyl radical combustion was observed. This aspect paves the way for an optimized implementation of kinetic mechanisms in CFD analysis devoted to the characterization of reactive systems involving a wide range of components. Indeed, this work demonstrates that it is possible to merge the common approach identifying the key elements in solid and liquid degradation processes with gas-phase detailed kinetics, debottlenecking the detailed characterization of industrial systems potentially interested by a degradative process and fire accidents.

CRediT authorship contribution statement

Benedetta Anna De Liso: Writing – original draft, Visualization, Software. **Gianmaria Pio:** Writing – review & editing, Supervision, Methodology, Investigation, Conceptualization. **Ernesto Salzano:** Writing – review & editing, Supervision, Project administration.

Declaration of competing interest

The authors declare that they have no known competing financial interests or personal relationships that could have appeared to influence the work reported in this paper.

Acknowledgement

Funding received from the Italian Ministry of University and Research under the National Recovery and Resilience Plan, Misson 4, Component 2, NextGenerationEU, Project “Network 4 Energy Sustainable Transition”, PE00000021, CUPJ33C22002890007 and project ECOSISTER-Ecosystem for Sustainable Transition Code ECS00000033, CUP J33C22001240001 are gratefully acknowledged.

Data availability

Data will be made available on request.

References

[1] Bozzano G, Manenti F. Efficient methanol synthesis: Perspectives, technologies and optimization strategies. Prog Energy Combust Sci 2016;56:71–105. https://doi.org/10.1016/j.pecs.2016.06.001.
[2] Gupta AK, Ibrahim S, Al SA. Advances in sulfur chemistry for treatment of acid gases. Prog Energy Combust Sci 2016;54:65–92. https://doi.org/10.1016/j.pecs.2015.11.001.
[3] Niermann M, Beckendorff A, Kaltschmitt M, Bonhoff K. Liquid Organic Hydrogen Carrier (LOHC) – Assessment based on chemical and economic properties. Int J Hydrogen Energy 2019;44:6631–54. https://doi.org/10.1016/j.ijhydene.2019.01.199.
[4] Sileghem L, Alekseev VA, Vancoillie J, Van Geem KM, Nilsson EJK, Verhelst S, et al. Laminar burning velocity of gasoline and the gasoline surrogate components iso-octane, n-heptane and toluene. Fuel 2013;112:355–65. https://doi.org/10.1016/j.fuel.2013.05.049.
[5] Violi A, Yan S, Eddings EG, Sarofim AF, Granata S, Faravelli T, et al. Experimental formulation and kinetic model for JP-8 surrogate mixtures. Combust Sci Technol 2002. https://doi.org/10.1080/00102200215080.
[6] Chang JI, Lin C-C. A study of storage tank accidents. J Loss Prev Process Ind 2006;19:51–9. https://doi.org/10.1016/j.jlp.2005.05.015.
[7] Barjoee SS, Elmi MR, Varaoon VT, Keykhosravi SS, Karimi F. Hazards of toluene storage tanks in a petrochemical plant: modeling effects, consequence analysis, and

comparison of two modeling programs. Environ Sci Pollut Res 2022;29:4587–615. https://doi.org/10.1007/s11356-021-15864-5.
[8] OSHA. Occupational Safety and Health Administration 2023. https://www.osha.gov/ords/imis/accidentsearch.html.
[9] García A, Pastor JV, Monsalve-Serrano J, Iñiguez E. Detailed assessment of exhaust emissions in a diesel engine running with low-carbon fuels via FTIR spectroscopy. Fuel 2024;357:129707. https://doi.org/10.1016/j.fuel.2023.129707.
[10] Ji C, Egolfopoulos FN. Flame propagation of mixtures of air with binary liquid fuel mixtures. Proc Combust Inst 2011. https://doi.org/10.1016/j.proci.2010.06.085.
[11] da Silva RM, Lang R, Thion S, Nmira F, Consalvi JL. Experimental study of the thermal and burning characteristics of 15 cm pool fires fueled by heptane-toluene mixtures. Int J Therm Sci 2023;193:108454. https://doi.org/10.1016/j.ijthermalsci.2023.108454.
[12] Sharma A, Vishwakarma PK, Mishra S, Mishra KB. Visible length and thermal radiation of WCO biodiesel and ethanol pool fires. Fuel 2020;280:118396. https://doi.org/10.1016/j.fuel.2020.118396.
[13] Rengel B, Mata C, Pastor E, Casal J, Planas E. A priori validation of CFD modelling of hydrocarbon pool fires. J Loss Prev Process Ind 2018;56:18–31. https://doi.org/10.1016/j.jlp.2018.08.002.
[14] Spinti JP, Thornock JN, Eddings EG, Smith PJ, Sarofim AF. Heat transfer to objects in pool fires. Dev. Heat Transf., vol. 20. 1st ed., New Forest National Park, UK: WIT Press; 2008, p. 69–136. https://doi.org/10.2495/978-1-84564-160-3/03.
[15] Hottel HC. Review of certain laws governing diffusive burning of liquids. Fire Res Abstr Rev 1959;1.
[16] Chen Y, Fang J, Zhang X, Miao Y, Lin Y, Tu R, et al. Pool fire dynamics: Principles, models and recent advances. Prog Energy Combust Sci 2023;95:101070. https://doi.org/10.1016/j.pecs.2022.101070.
[17] Zukoski EE, Cetegen BM, Kubota T. Visible structure of buoyant diffusion flames. Symp Combust 1985;20:361–6. https://doi.org/10.1016/S0082-0784(85)80522-1.
[18] Thomas PH. The size of flames from natural fires. Symp Combust 1963;9:844–59. https://doi.org/10.1016/S0082-0784(63)80091-0.
[19] Heskestad G. Fire plumes, flame height, and air entrainment. SPFE Handb Fire Prot Eng 2002.
[20] McCaffrey BJ. Purely Buoyant Diffusion Flames (NBSIR 791910); 1979.
[21] Bariha N, Srivastava VC, Mishra IM. Theoretical and experimental studies on hazard analysis of LPG/LNG release: A review. Rev Chem Eng 2017;33:387–432. https://doi.org/10.1515/revce-2016-0006.
[22] Klassen M, Gore JP, Sivathanu YR, Hamins A, Kashiwagi T. Radiative heat feedback in a toluene pool fire. Symp Combust 1992;24:1713–9. https://doi.org/10.1016/S0082-0784(06)80200-6.
[23] De Liso BA, Pio G, Salzano E. Fire behaviour of liquid solvents for energy storage applications. Process Saf Environ Prot 2024;188:726–34. https://doi.org/10.1016/j.psep.2024.05.153.
[24] De Liso BA, Pio G, Salzano E. Small scale pool fires: The case of toluene. J Loss Prev Process Ind 2024;92:105430. https://doi.org/10.1016/j.jlp.2024.105430.
[25] Shen R, Jiao Z, Parker T, Sun Y, Wang Q. Recent application of Computational Fluid Dynamics (CFD) in process safety and loss prevention: A review. J Loss Prev Process Ind 2020;67:104252. https://doi.org/10.1016/j.jlp.2020.104252.
[26] Lu T, Law CK. Toward accommodating realistic fuel chemistry in large-scale computations. Prog Energy Combust Sci 2009;35:192–215. https://doi.org/10.1016/j.pecs.2008.10.002.
[27] Egolfopoulos FN, Hansen N, Ju Y, Kohse-Hoinghaus K, Law CK, Qi F. Advances and challenges in laminar flame experiments and implications for combustion chemistry. Prog Energy Combust Sci 2014;43:36–67. https://doi.org/10.1016/j.pecs.2014.04.004.
[28] Lin KC, Lee TW. Skeletal mechanism of ethyl propionate oxidation for CFD modeling to predict experimental profiles of unsaturated products in a nonpremixed flame. Energy Fuel 2018;32:855–66. https://doi.org/10.1021/acs.energyfuels.7b02809.
[29] Quan Y, Zhang Z, Tanchak RN, Wang Q. A review on cone calorimeter for assessment of flame-retarded polymer composites. J Therm Anal Calorim 2022;147:10209–34. https://doi.org/10.1007/s10973-022-11279-7.
[30] Bray RJ, Tretsiakova-McNally S, Zhang J. The controlled atmosphere cone calorimeter: a literature review. Fire Technol 2023. https://doi.org/10.1007/s10694-023-01423-6.
[31] Mun SY, Cho JH, Hwang CH. Effects of external heat flux and exhaust flow rate on co and soot yields of acrylic in a cone calorimeter. Appl Sci 2021;11. https://doi.org/10.3390/app11135942.
[32] De Liso BA, Pio G, Salzano E. Multicriteria approach to assess the fire behaviour of polymers in electrochemical energy storage. J Loss Prev Process Ind 2025;94:105541. https://doi.org/10.1016/j.jlp.2024.105541.
[33] Marsh ND, Gann RG. Smoke component yields from Bench-Scale Fire Tests : 3. ISO 5660-1 / ASTM E 1354 with Enclosure and Variable Oxygen Concentration. Gaithersburg, MD; 2013. https://doi.org/10.6028/NIST.TN.1762.
[34] McGrattan K, Hostikka S, McDermott R, Floyd J, Weinschenk C, Overhold K. Fire dynamics simulator (FDS) validation technical reference guide volume 3 : Validation. NIST Spec Publ 2019;1018:3. https://doi.org/10.6028/NIST.SP.1018-1.
[35] McGrattan K, Hostikka S, Floyd J, McDermott R, Vanella M, Mueller E. Fire Dynamics Simulator (Version 6.8.0), Technical Reference Guide 2023;1.
[36] Hostikka S, McGrattan K, McDermott R, Floyd J, Overholt K, Weinschenk C. Fire Dynamics Simulator Technical Reference Guide Volume 1: Mathematical Model 2015;6.3.0. https://doi.org/10.6028/NIST.SP.1018-1.
[37] Pio G, Carboni M, Salzano E. Realistic aviation fuel chemistry in computational fluid dynamics. Fuel 2019;254:115676. https://doi.org/10.1016/j.fuel.2019.115676.
[38] Carboni M, Pio G, Mocellin P, Vianello C, Maschio G, Salzano E. On the flash fire of stratified cloud of liquefied natural gas. J Loss Prev Process Ind 2022;75:104680. https://doi.org/10.1016/j.jlp.2021.104680.
[39] Liu C, Jangi M, Ji J, Yu L, Ding L. Experimental and numerical study of the effects of ullage height on plume flow and combustion characteristics of pool fires. Process Saf Environ Prot 2021;151:208–21. https://doi.org/10.1016/j.psep.2021.04.040.
[40] Huang P, Zhang R, Yu L, Liu C. Study on the combustion, entrainment, and plume flow behaviors of annular pool fires. Environ Sci Pollut Res 2023;30:59781–92. https://doi.org/10.1007/s11356-023-26748-1.
[41] Montgomery MJ, Das DD, McEnally CS, Pfefferle LD. Analyzing the robustness of the yield sooting index as a measure of sooting tendency. Proc Combust Inst 2019;37:911–8. https://doi.org/10.1016/j.proci.2018.06.105.
[42] Sunderland PB, Faeth GM. Soot formation in hydrocarbon air laminar jet diffusion flames. Combust Flame 1996;105:132–46. https://doi.org/10.1016/0010-2180(95)00182-4.
[43] Di Blasi C. Modeling chemical and physical processes of wood and biomass pyrolysis. Prog Energy Combust Sci 2008;34:47–90. https://doi.org/10.1016/j.pecs.2006.12.001.
[44] Pio G, Dong X, Salzano E, Green WH. Automatically generated model for light alkene combustion. Combust Flame 2022;241:112080. https://doi.org/10.1016/j.combustflame.2022.112080.
[45] Dong X, Pio G, Arafin F, Laich A, Baker J, Ninnemann E, et al. Butyl acetate pyrolysis and combustion chemistry: mechanism generation and shock tube experiments. J Phys Chem A 2023;127:3231–45. https://doi.org/10.1021/acs.jpca.2c07545.